[PROC. OF JSCE No. 426/V-14 (Concrete Eng. and Pavements) February 1991]

DEFORMATIONAL COMPATIBILITY FOR SOLID PHASE OF DENSE LIQUID-SOLID FLOW IN BEND PIPES

By Anura NANAYAKKARA, Kazumasa OZAWA** and Koichi MAEKAWA****

The objective of this research is to establish the deformational compatibility for aggregate phase of concrete in bend pipes used for concrete pumping. The deformational compatibility, which describes the relationship between the strain rate of aggregate phase (particle assembly) developing over a reference section and sectional mean flow speed of the particle assembly, is essential in one-dimensional computation of dense liquid-solid flow in pipe lines. Flow visualization and image processing on model concrete were carried out for development of the mathematical description of the deformational compatibility for aggregate phase in bend pipes, in which the second strain invariant of aggregate phase was adopted as a main parameter associated with stress generation due to particle-to-particle interactions. The authors have proposed a simplified compatibility formulation reduced to one-dimensional condition and applicable to dense liquid-solid flow in bend pipe portions, by relating the sectional averaged invariant of strains to the mean flow speed of solid phase and the curvature of bend pipes.

Keywords: *solid-liquid flow, bend pipe, deformational compatibility, pumpability, multi-phase flow*

1. INTRODUCTION

The bend pipe is an essential part not only in concrete pumping pipeline networks but also in truck mounted concrete pumps with booms. It gives rise to higher pressure drop and sometimes blocking specially with low slump concrete[1] or stiffened concrete due to time-dependent loss of slump. The pressure drop in bend and tapered pipes depends not only on the dimensions of the pipes such as radius of curvature in bend pipes, tapered angle and diameter, but also on the mix proportion of fresh concrete. The response of each part (i.e. bend and tapered pipes) may be different for different types of mix proportion of concrete. For example, fresh concrete with low segregation resistance has a higher risk of blocking in tapered pipes than in bend pipes. On the other hand, the risk of blocking may be higher for bend pipes than for tapered ones in case of stiff concrete mixes. In spite of these differences with regard to tapered and bend pipes, it is recommended in the "Recommended Practice for Pumping"[2] that the pressure drop for bend pipe is twice that of tapered pipe for whatever the mix proportion and also without paying much attention to dimension of each individual part. Therefore, it is necessary to study the deformation of fresh concrete in bend and tapered pipes in order to evaluate pumpability of fresh concrete for a given pipe line.

For evaluation of pumpability, the authors have adopted the multi-phase (i.e. aggregate, sand and paste phases) concept[3)~5)] which can treat transient segregation and flow resistance simultaneously. To apply this model to bend pipes, it is necessary to find out the deformational compatibility of aggregate phase for bend pipes which relates the strain rate over a flow section and flow speed of aggregate including dimensions of the pipe.

* Member of JSCE, Dr. Eng., Lecturer, Dept. of Civil Engineering, University of Moratuwa, Srilanka
** Member of JSCE, Ms. Eng., Assistant Lecturer, Dept. of Civil Engineering, University of Tokyo
*** Member of JSCE, Dr. Eng., Associate Professor, Dept. of Civil Engineering, University of Tokyo

In order to obtain the deformational characteristics of solid phase in the dense liquid-solid flow through tapered and bifurcations[6),7)] flow visualization had been successfully applied and based on that, the authors have established the simplified deformational compatibility for tapered pipes[7)]. This paper reports the evaluation of the deformational compatibility for bend pipes by using the same procedure.

2. DEFORMATIONAL COMPATIBILITY ALONG THE AXIS OF THE BEND PIPE

To obtain the movement of particle assembly, there exist analytical procedures to treat every particle individually[8)-10)]. The other approach which the authors have adopted, treats the particle assembly as a continuous media with spatially averaged flow vectors. The latter approach makes it possible to use multi-phase mechanics in analyzing the liquid-solid flow incorporating segregation between solid and liquid. Here the spatially averaged flow vector $\vec{V}$ of aggregate phase at any location expressed by $\vec{r}$ is given in the cylindrical coordinate system as,

$$\vec{V}=(u_r, u_\theta, u_z)=\vec{V}(\vec{r}, t)=\frac{\int_{v_c}\vec{v}(\vec{r}+\vec{r'}, t)\rho(\vec{r}+\vec{r'}, t)dv}{\int_{v_c}\rho(\vec{r}+\vec{r'}, t)dv} \quad \cdots\cdots (1)$$

where $\vec{r'}$ is incremental position vector defined in the integral volume v_c with the origin denoted by $\vec{r}$ where $\vec{r'}=0$, and $\vec{v}(\vec{r}+\vec{r'})$ is the velocity vector defined on the particles and $\rho(\vec{r}+\vec{r'})$ is equal to unity when position vector $(\vec{r}+\vec{r'})$ is included in a solid particle, otherwise, $\rho(\vec{r}+\vec{r'})$ is zero as shown in Fig. 1. In this paper, the integral volume v_c is named control volume including several particles[7)] and the center location is denoted by $\vec{r}$ as shown in Fig. 1.

The spatially averaged strain field in three dimensional flowing condition is represented by the gradient of flow vector $\vec{V}$ in cylindrical coordinate system as,

$$\begin{aligned}\mathrm{grad}\,\vec{V}=&\frac{\partial u_r}{\partial r}(e_1; e_1)+\frac{\partial u_\theta}{\partial r}(e_1; e_2)+\frac{\partial u_z}{\partial r}(e_1; e_3)+\frac{1}{r}\left(\frac{\partial u_r}{\partial \theta}-u_\theta\right)(e_2; e_1)\\&+\frac{1}{r}\left(\frac{\partial u_\theta}{\partial \theta}+u_r\right)(e_2; e_2)+\frac{1}{r}\left(\frac{\partial u_z}{\partial \theta}-u_\theta\right)(e_2; e_3)+\frac{\partial u_r}{\partial z}(e_3; e_1)\\&+\frac{\partial u_\theta}{\partial z}(e_3; e_2)+\frac{\partial u_z}{\partial z}(e_3; e_3) \quad \cdots\cdots (2)\end{aligned}$$

where, e_1, e_2 and e_3 are unit base vectors in r, θ and z directions and $(e_i; e_j)$ is dyadic multiplication in tensor symbolic notation. The sectional averaged stress σ_a of aggregate phase as shown in Fig. 2 must be a function of grad $\vec{V}$ as,

$$\sigma_a=\frac{1}{A}\int_A \sigma(\mathrm{grad}\,\vec{V})dA \quad \cdots\cdots (3)$$

where σ is the constitutive law for axial stress evaluation due to particle to particle interaction and A is

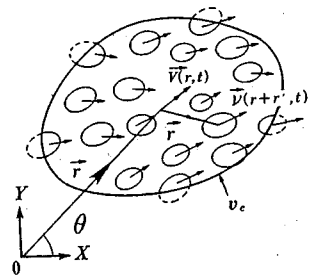

Fig. 1 Definition sketch of position vectors and control volume v_c[7)].

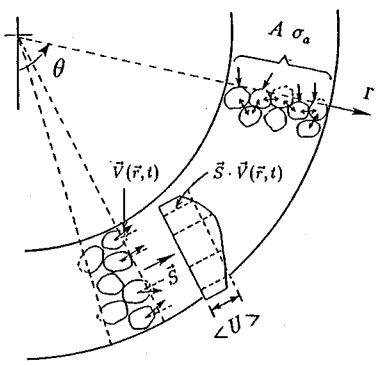

Fig. 2 Sectional averaged circumferential velocity $\langle U\rangle$ and averaged contact stress σ_a.

the sectional area of the pipe. This kind of approach is possible only when we have the continuous strain field. As the one dimensional flow analysis along the pipe axis (the main stream line) is concerned, we have only the sectional averaged flow speed $\langle U\rangle$ in the circumferential direction as defined in Eq. (4) and illustrated in Fig. 2.

$$\langle U\rangle=\frac{1}{A}\int_A \vec{V}(\vec{r})\cdot\vec{S}\,dA \quad (4)$$

where $\vec{S}$ is the unit vector oriented in the circumferential direction of pipe. Since we have only the sectional averaged flow rate, the approach similar to the reduced compatibility in classical beam theory based on Euler-Kirchoff hypothesis has been adopted to obtain the deformational compatibility which can be used to evaluate the sectional stress in one dimensional flow analysis of dense liquid-solid materials[7].

There exists three modes of deformation[13] expressed by the general gradient of flow field in Eq. (2), that is, shear mode denoted by 'J', volumetric mode denoted by 'I' and spin mode expressed by ω. In case of two dimensional space denoted by (r, θ), where the flow visualization test is conducted, we have

$$I=\frac{\epsilon_{rr}+\epsilon_{\theta\theta}}{2} \quad (5)$$

$$J=\sqrt{\left(\frac{\epsilon_{rr}-\epsilon_{\theta\theta}}{2}\right)^2+\epsilon_{r\theta}^2} \quad (6)$$

$$\omega=\left(\frac{\partial u_\theta}{\partial r}-\frac{1}{r}\frac{\partial u_r}{\partial\theta}+\frac{u_\theta}{r}\right) \quad (7)$$

where

$$\epsilon_{rr}=\frac{\partial u_r}{\partial r} \qquad (e_1\,;\,e_1)\ \text{component} \quad (8)$$

$$\epsilon_{\theta\theta}=\frac{1}{r}\frac{\partial u_\theta}{\partial\theta}+\frac{u_r}{r} \qquad (e_2\,;\,e_2)\ \text{component} \quad (9)$$

$$\epsilon_{r\theta}=\frac{1}{2}\left(\frac{1}{r}\frac{\partial u_r}{\partial\theta}+\frac{\partial u_\theta}{\partial r}-\frac{u_\theta}{r}\right) \qquad (e_1\,;\,e_2)\ \text{and}\ (e_2\,;\,e_1)\ \text{component} \quad (10)$$

Special attention has been paid to the invariant J since stress generation due to particle to particle collision and friction is related to shear mode of deformation[6] [11]

3. DEFORMATION OF SOLID PHASE IN DENSE LIQUID-SOLID FLOW IN BEND PIPES

(1) Visual test

The authors used model mortar which was invented by Hashimoto *et al.* [12] in the same way it has been used in tapered pipes[7]. The apparatus as shown in Fig. 3 was used to reproduce the two dimensional motion of particles in bend pipes as the first step to approach the general three dimensional motion of particles. Model concrete[13] consists of transparent polymer media (model mortar) and plastic spheres (25 mm in diameter) has been used to reproduce flow pattern of particles in a dense liquid-solid media in bend pipes. As experimental parameters, the radius of curvature of the bend, flow speed, viscosity of model mortar and particle contact condition have been selected. The test series conducted are given in Table 1.

(2) Lagrangian evaluation of aggregate phase

Fig. 4 shows the traces of two adjacent rows of particles at constant time intervals for different particle contact conditions. In the case of loosely arranged condition with less particle interaction (test BHH of Table 1), the inner and outer layers of particles seem to have the same velocity which results in the re-arrangement of particle assembly in the cylindrical coordinate system. This is further clarified by Fig. 5 which shows nearly constant angular velocity distribution across the pipe section. In the case of closely pack arrangement (test CHH of Table 1), the particles' re-arrangement is small in appearance as a Lagrangian expression and rows of particles are trying to maintain the radial line, but as shown in Fig. 6,

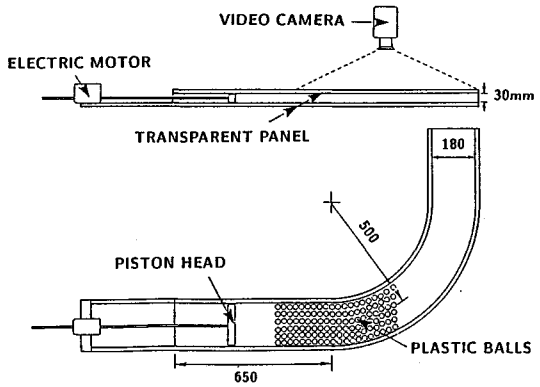

Fig. 3 Pumping apparatus for visual test.

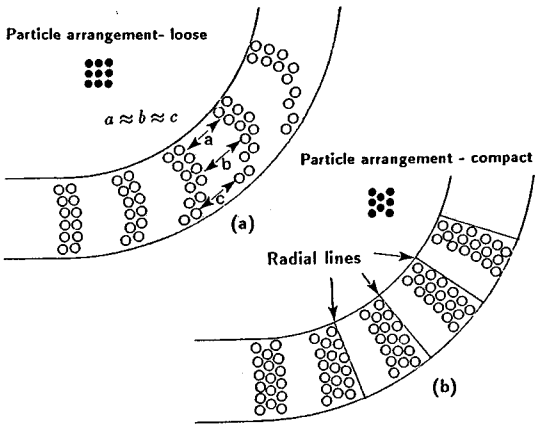

Fig. 4 Lagrangian traces of particles.

Table 1 Test series.

Test	Particle* arrangement	Viscosity** of liquid	Radius of bend(cm.)	Averaged flow speed(cm/s)
BHH	L	H	50	4.62
BLH	L	L	50	4.28
CHH	C	H	50	4.19
CLH	C	L	50	4.44
GHM	L	H	50	2.78
FHM	C	H	50	3.12
DLL	L	L	50	2.22
ELL	C	L	50	1.89
DHL	L	H	50	2.26
EHL	C	H	50	2.16
1HH	L	H	25	4.53
2HH	C	H	25	4.38
3HL	L	H	25	2.09
4HL	C	H	25	2.03
5HH	L	H	25	3.26
6HH	C	H	25	3.19

* L - Loose - corresponding volume fraction is 37.4%
C - Compact - corresponding volume fraction is 40.1%
** L - low viscosity - " P " funnel time is 4 mts 15 sec.
H - High viscosity - " P " funnel time is 12 mts.

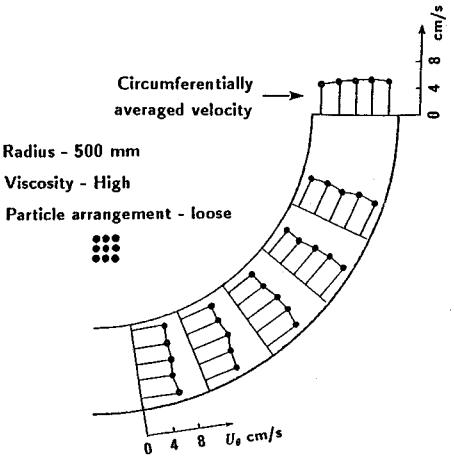

Fig. 5 Sectional velocity distribution for loosely arranged particles.

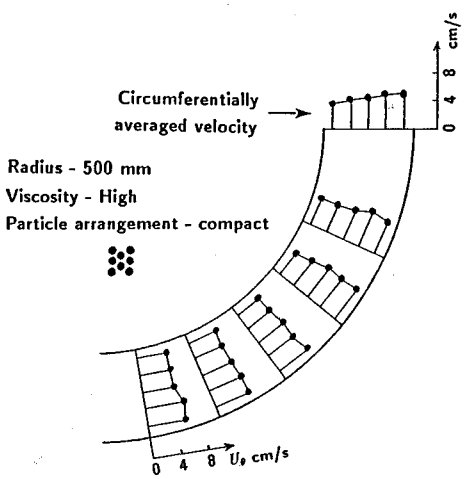

Fig. 6 Sectional velocity distribution for closely packed arranged particles.

the velocity distribution which is so-called Eulerian expression is similar to the one shown in Fig. 5. Even though particles are interlocked against adjacent layers to restrain the relative movement in the circumferential direction to a considerable extent, there still exists deformation in the circumferential direction with respect to the radial line.

(3) Image data processing and flow pattern

Based on the visual image data of model concrete, the spatial averaging method for motion of particle assembly was used based on Eulerian expression[13]. In this case the visual image is divided into radial elements as shown in Fig. 7 and the rest of the process of image analysis is carried out similar to the tapered pipe[6),7),13)]. The integration of velocity in Eq. (4) was numerically carried out to create Eulerian continuous velocity field as shown in Fig. 8. Even in both loose and compact arrangements of test 3 HH and 4 HH in Table 1, smooth flow of particles can be seen in Fig. 9 and Fig. 10, which is due to nonexistence of radial deformation. But in the case of tapered pipe, re-arrangement of particles takes place and the flow line of particles will mix in the tapered section[7]. According to the sectional distribution of velocity (Fig. 5 and Fig. 6), the nearly uniformly distributed circumferential velocity is observed despite of particle arrangement. In the case of bend with small radius (25 cm) the sectional distribution of velocity is fairly uniform for both compact (test 4 HL in Table 1 and shown in Fig. 11) and loose (test 3 HL in Table 1 and shown in Fig. 12) arrangement of particles. In the case of loose arrangement the maximum velocity of each section is somewhere close to the inner side of the pipe while in the case of compact arrangement it is always at the outer most layer as indicated in Fig. 11 and Fig. 12. In this type of flow pattern, the only possible deformation mode is pure shear deformation which will be further clarified by using the strain distributions.

(4) Two dimensional strain field and invariants

To eliminate image scanning errors, according to data processing technique, the time averaged strains $\overline{\epsilon_{rr}}$, $\overline{\epsilon_{\theta\theta}}$ and $\overline{\epsilon_{r\theta}}$ were obtained from the time averaged velocity field $\overline{u_i}$ as given below[13].

$$\overline{\epsilon_{rr}}=\frac{\partial \overline{u_r}}{\partial r} \quad \cdots\cdots (11)$$

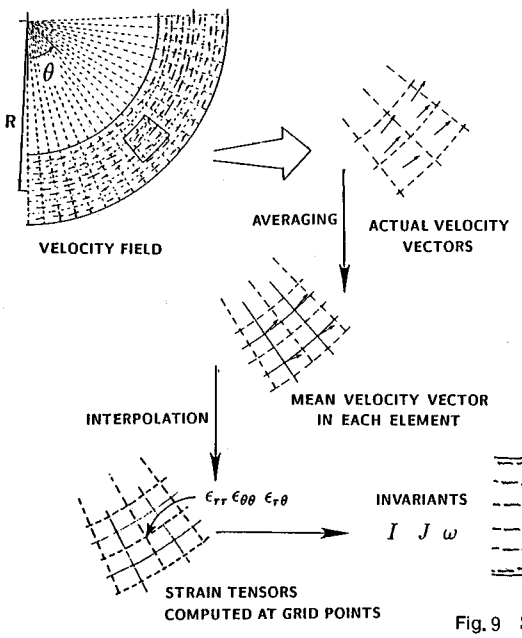

Fig. 7 Spatial averaging procedure.

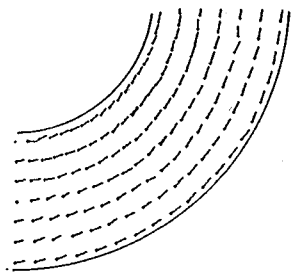

Fig. 8 Generated continuous velocity field.

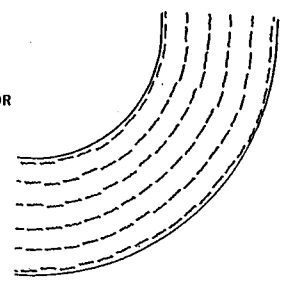

Fig. 9 Stream lines of particles for loosely arranged particles.

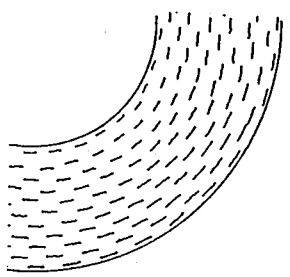

Fig. 10 Stream lines of particles for closely packed particle arrangement.

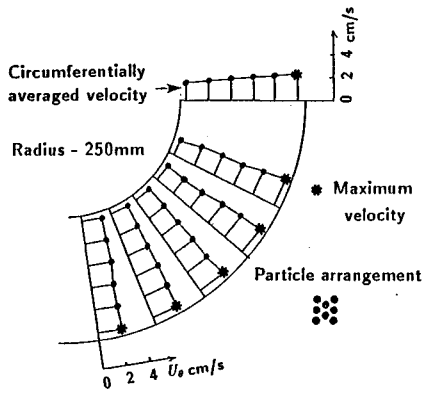

Fig. 11 Sectional distribution of circumferential velocity for compact arrangement of particles.

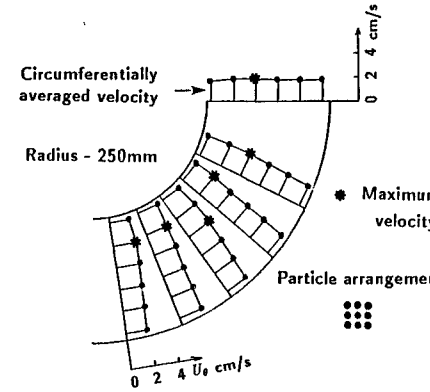

Fig. 12 Sectional distribution of circumferential velocity for loosely arranged particles.

$$\overline{\epsilon_{\theta\theta}}=\frac{1}{r}\frac{\partial \overline{u_\theta}}{\partial \theta}+\frac{\overline{u_r}}{r} \quad \cdots\cdots (12)$$

$$\overline{\epsilon_{r\theta}}=\frac{1}{2}\left(\frac{1}{r}\frac{\partial \overline{u_r}}{\partial \theta}+\frac{\partial \overline{u_\theta}}{\partial r}-\frac{\overline{u_\theta}}{r}\right) \quad \cdots\cdots (13)$$

The distribution of $\overline{\epsilon_{rr}}$, $\overline{\epsilon_{\theta\theta}}$ and $\overline{\epsilon_{r\theta}}$ for selected sections (test 3 HL in Table 1) are shown in Fig. 13. As expected, it can be seen in Fig. 13 that $\overline{\epsilon_{rr}}$ and $\overline{\epsilon_{\theta\theta}}$ are relatively small and shear strain $\overline{\epsilon_{r\theta}}$ is distinct compared with $\overline{\epsilon_{rr}}$ and $\overline{\epsilon_{\theta\theta}}$. In this kind of deformation mode, that is pure shear deformation with zero circumferential and radial deformation, the principal directions of the aggregates' strains are at 45° to the axis of the pipe. When we compare the strain distribution of tapered pipe (Fig. 14) with the one in bend pipe, shear strain ($\overline{\epsilon_{xy}}$) along the axis of tapered pipes is on the contrary negligible. Furthermore, the radial stain is approximately equal and opposite to the axial strain, and under this type of deformational mode, the principal strain direction coincides with the pipe axis. As far as the deformational mode is concerned, both bend and tapered pipes have pure shear deformation but their principal directions differ each other by 45°.

Sectional distribution of time averaged invariants $\overline{I}$ and $\overline{J}$ (test 3 HL of Table 1) are shown in Fig. 15. The invariant $\overline{I}$ is almost zero which implies that there is no segregation of particles as expected in bend pipes. In other tests with different bend radius, flow speed and viscosity of liquid we had the same conclusion.

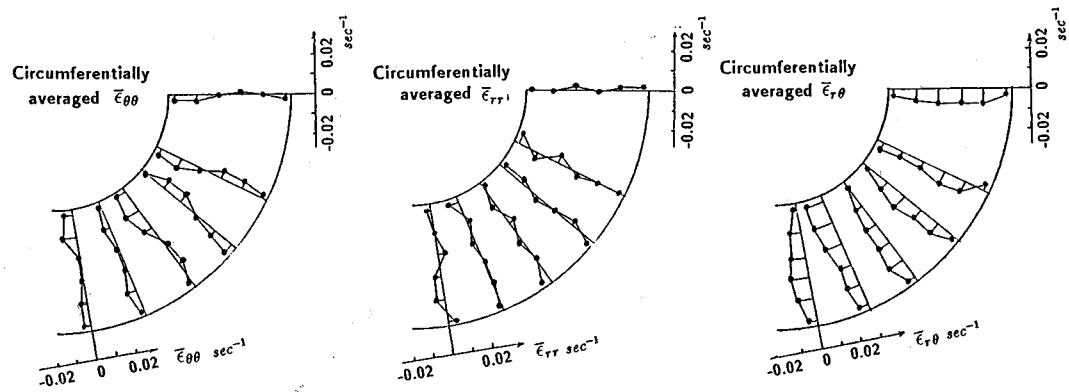

R = 250 mm Viscosity - High Particle arrangement - loose

Fig. 13 Sectional distribution of strains $\overline{\epsilon_{rr}}$, $\overline{\epsilon_{r\theta}}$, $\overline{\epsilon_{\theta\theta}}$.

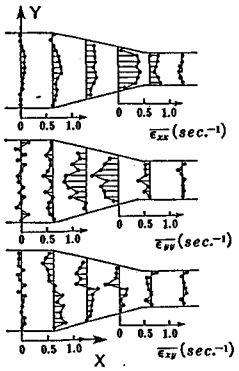

Fig. 14 Sectional distribution of strains $\overline{\epsilon_{xx}}$, $\overline{\epsilon_{yy}}$ and $\overline{\epsilon_{xy}}$[7].

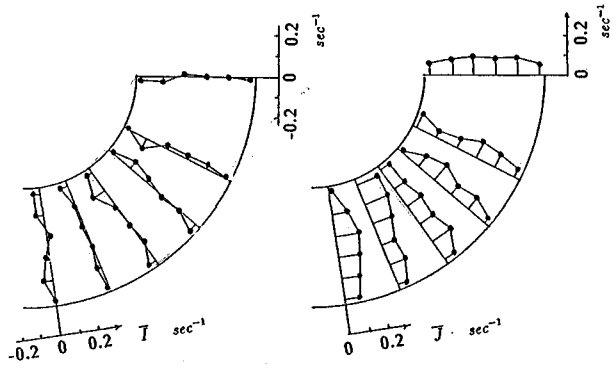

Fig. 15 Sectional distribution of strain invariant $\bar{I}$ and $\bar{J}$.

As for tapered pipes[7], it is intended to obtain one dimensional reduced compatibility relationship which can be combined with appropriate constitutive model to calculate axial force of aggregate phase in bend pipes. Fig. 16 shows the experimentally obtained sectional averaged values of invariants $\langle\bar{I}\rangle$ and $\langle\bar{J}\rangle$ by using the same procedure in reference[7]. As described earlier, we can see that $\langle\bar{J}\rangle$ is fairly constant along the pipe axis with respect to θ and $\langle\bar{I}\rangle$ is nearly zero which indicates pure shear deformation. According to Fig. 17, it can be noted that there is no noticeable influence on $\langle\bar{J}\rangle$ due to change in viscosity of liquid. The circumferentially averaged value of $\langle\bar{J}\rangle$ can be used to represent the shear deformation regardless to θ since the $\langle\bar{J}\rangle$ is nearly constant along the bend portion. Then, the main point of discussion, the prediction of the value $\langle\bar{J}\rangle$ in any kind of flow boundary condition and material mix proportion, is discussed in the next chapter.

4. A PROPOSAL OF REDUCED COMPATIBILITY FOR BEND PIPE IN TWO DIMENSION

The final aim of this section is to formulate the relationship between the sectional averaged $\langle\bar{J}\rangle$ and the mean flow rate $\langle\bar{U}\rangle$ including the dimension of the pipe. Exact two-dimensional compatibility gives us the following expression by substituting appropriate strains from Eq. (2) into Eq. (6) as,

$$\langle\bar{J}\rangle=\frac{1}{A}\int_A\overline{J(r,\theta,z)}drdz \qquad (dA=drdz)$$

$$=\frac{1}{A\Delta t}\int_t^{t+\Delta t}\int_A\left(\sqrt{\left(\frac{\epsilon_{rr}-\epsilon_{\theta\theta}}{2}\right)^2+\epsilon_{r\theta}^2}\right)dtdA$$

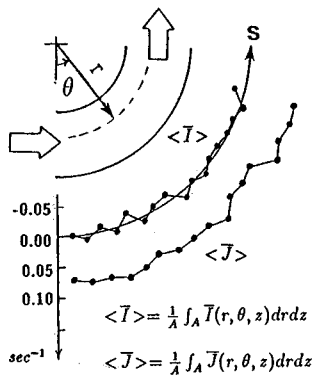

Fig. 16 Definition and distribution of sectional averaged $\langle\bar{I}\rangle$ and $\langle\bar{J}\rangle$.

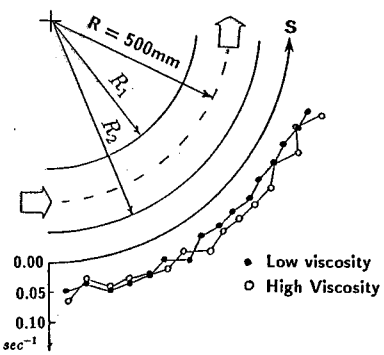

Fig. 17 Distribution of $\langle\bar{J}\rangle$ for two different viscosities.

$$=\frac{1}{A\Delta t}\int_t^{t+\Delta t}\int_A |\epsilon_{r\theta}|\sqrt{1+\phi^2}\,dtdA \quad (14)$$

where

$$\phi=\frac{\epsilon_{rr}-\epsilon_{\theta\theta}}{2\,\epsilon_{r\theta}}=\frac{\epsilon_{rr}-I}{\epsilon_{r\theta}} \quad (15)$$

We have a Taylor expansion with respect to parameter ϕ as

$$\langle\bar{J}\rangle=\frac{1}{A\Delta t}\int_t^{t+\Delta t}\int_A |\epsilon_{r\theta}|\left(1+\underbrace{\frac{\phi^2}{2}-\frac{\phi^4}{8}+\frac{\phi^6}{16}\cdots}_{\text{higher order terms}}\right)dtdA \quad (16)$$

$$\langle\bar{J}\rangle=\langle\bar{J}_{1st}\rangle+J_h(\phi) \quad (17)$$

$$\langle\bar{J}_{1st}\rangle=\frac{1}{A\Delta t}\int_t^{t+\Delta t}\int_A |\epsilon_{r\theta}|\,dtdA=\frac{1}{A}\int_A |\overline{\epsilon_{r\theta}}|\,dA \quad (18)$$

$$J_h(\phi)=\frac{1}{A\Delta t}\int_t^{t+\Delta t}\int_A |\epsilon_{r\theta}|\left(\underbrace{\frac{\phi^2}{2}-\frac{\phi^4}{8}+\frac{\phi^6}{16}\cdots}_{\text{higher order terms}}\right)dtdA \quad (19)$$

where $\langle\bar{J}_{1st}\rangle$ and $J_h(\phi)$ are first order and higher order components of strain invariant $\langle\bar{J}\rangle$ respectively.

The object of this paper is to empirically find the relation of $\langle\bar{J}\rangle$ and the mean flow $\langle\bar{U}\rangle$ as Eq. (4). Here, let us focus our attention on the first order term in Eq. (16), because the higher order terms with respect to ϕ can be expected to be small compared with the first linear term. This assumption of linearity will be verified in this section. In the steady state flow, there exists the exact solution of the first order compatibility $\langle\bar{J}_{1st}\rangle$ in Eq. (18). Substituting the expression for $\overline{\epsilon_{r\theta}}$ from Eq. (13) into Eq. (18), we have,

$$\langle\bar{J}_{1st}\rangle=\frac{1}{A}\int_A\frac{1}{2}\left|\frac{1}{r}\frac{\partial\bar{u}_r}{\partial\theta}+\frac{\partial\bar{u}_\theta}{\partial r}-\frac{\bar{u}_\theta}{r}\right|dA \quad (20)$$

The first two terms, i. e. $\frac{1}{r}\frac{\partial\bar{u}_r}{\partial\theta}$ and $\frac{\partial\bar{u}_\theta}{\partial r}$, are neglected since the radial velocity $\bar{u}_r$ is almost zero and the circumferential velocity $\bar{u}_\theta$ is nearly constant across the pipe section as discussed in chapter 3. Then we have,

$$\langle\bar{J}_{1st}\rangle=\frac{1}{2}\frac{1}{A}\int_A\left|\frac{\bar{u}_\theta}{r}\right|dA=\frac{1}{2\,bd}\int_{R_1}^{R_2}\frac{\bar{u}_\theta}{r}\,bdr=\frac{1}{2\,d}\left([\bar{u}_\theta\cdot\ln(r)]_{R_1}^{R_2}-\int_{R_1}^{R_2}\ln(r)\frac{\partial\bar{u}_\theta}{\partial r}\,dr\right) \quad (21)$$

where R_1 and R_2 are inner and outer radius of bend, b is the depth of bend and $d=R_2-R_1$ as shown in Fig. 17.

According to the visual test, the variation of circumferential velocity u_θ in the radial direction is negligible. Then we can assume that,

$$\frac{\partial\bar{u}_\theta}{\partial r}=0,\quad\text{and}\quad\langle\bar{U}\rangle=\frac{1}{A}\int\bar{u}_\theta dA\approx\bar{u}_\theta \quad (22)$$

By substituting the assumptions in Eq. (22) into Eq. (21), we have,

$$\langle\bar{J}_{1st}\rangle=\frac{1}{2}\langle\bar{U}\rangle\frac{1}{d}\ln\frac{R_2}{R_1} \quad (23)$$

When the mean radius R defined as $\frac{R_1+R_2}{2}$ is larger, $\frac{1}{d}\ln\frac{R_2}{R_1}$ is nearly equal to $\frac{1}{R}$. In the case of experimental boundary condition of $R=500$ mm and $d=180$ mm the error due to the above simplification is about 1% and in the case of $R=250$ mm it is about 4.7%. Then we can assume,

$$\langle\bar{J}_{1st}\rangle=\frac{1}{2}\frac{\langle\bar{U}\rangle}{R} \quad (24)$$

If the higher order terms in Eq. (16) is negligible, the expression of $\langle\bar{J}_{1st}\rangle$ in Eq. (24) becomes the reduced compatibility for bend pipes in two dimensional deformation.

The Fig. 18 shows the experimentally obtained shear intensity $\langle\bar{J}\rangle$ with respect to $\frac{\langle\bar{U}\rangle}{R}$ for two different radius of curvatures (i. e. $R=500$ mm and 250 mm), different flowing speeds (see Table 1) and also for

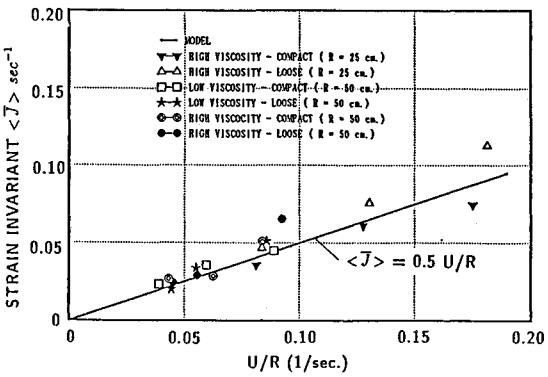

Fig. 18 Variation of $\langle \bar{J} \rangle$ vs. U/R.

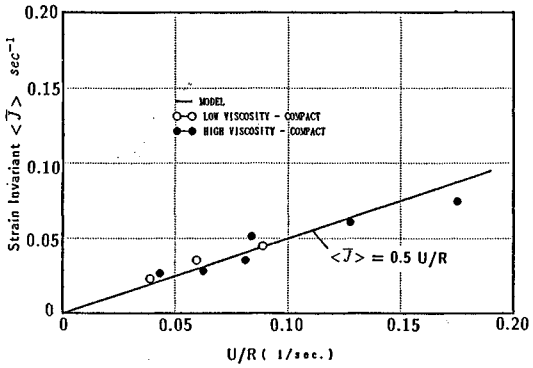

Fig. 19 Variation of $\langle \bar{J} \rangle$ vs. U/R for compact arrangement of particles.

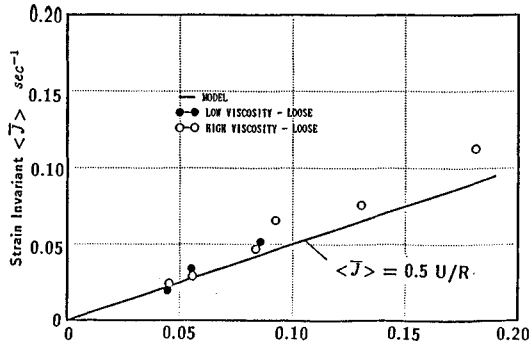

Fig. 20 Variation of $\langle \bar{J} \rangle$ vs. U/R for loosely arranged particles.

high and low viscosity of model mortar. It can be seen that the calculated values of $\langle \bar{J}_{1st} \rangle$ from Eq. (24) are close to the experimental results. It can be also seen that the effect of viscosity is hardly observed in both compact and loose arrangement of particles (see Fig. 19 and Fig. 20). According to Fig. 18, it seems that in case of bend pipes with greater curvature (R=25 cm) there is noticeable difference in $\langle \bar{J} \rangle$ with respect to particle arrangement. This is due to the existence of velocity gradient across the pipe section in case of compact particle arrangement which does not exist in the case of loose particle arrangement (Fig. 11 and Fig. 12). In other words, the higher order terms in Eq. (16) can not be neglected in the case of greater curvature but this kind of small bend pipes are not used in practice. Accordingly, it can be concluded that $\langle \overline{J_{1st}} \rangle$ calculated by Eq. (24) has a reasonable accuracy in the case of two dimensional deformation field corresponding to the actual boundary of pipe lines used in concrete pumping practice.

5. EXTENSION TO THREE DIMENSIONAL PIPE FLOW

The deformational compatibility given by Eq. (24) is applicable to two dimensional flow in rectangular ducts. However, piping used in concrete pumping is in circular shape in which flow of concrete is three dimensional. Even though three dimensional flowing condition in bend pipes is not axisymmetric, some of the assumptions used in two dimensional case can be extended to three dimensional case.

The intensity of shear deformation in three dimensional flow can be represented by the three dimensional second invariant J_{3D}[7] as,

$$J_{3D}=\sqrt{\frac{(\epsilon_\theta-I)^2}{2}+\frac{(\epsilon_r-I)^2}{2}+\frac{(\epsilon_z-I)^2}{2}+\epsilon_{r\theta}^2+\epsilon_{\theta z}^2+\epsilon_{zr}^2} \quad \cdots\cdots (25)$$

$$I=\frac{\epsilon_\theta+\epsilon_r+\epsilon_z}{3} \quad \cdots\cdots (26)$$

where ϵ_θ, ϵ_r, ϵ_z are strains in the direction of θ, r and z.

The radial, normal and axial strain ϵ_r, ϵ_z and ϵ_θ are expected to be small since the secondary or radial flow is considered to be negligible as in the two dimensional case due to high concentration of particles and non-existence of lateral deformation, because the pipe has uniform cross section unlike in tapered pipes. The circular bend pipe can be considered as the combination of rectangular ducts with mean radius R as shown in Fig. 21 according to the assumption of neglected secondary flow denoted by u_r and u_z. The only existing component of velocity is the circumferential speed u_θ with uniform distribution throughout the pipe section.

Similar to Eq. (16), an expression for $\langle\overline{J_{3D}}\rangle$ can be obtained from Eq. (25) as,

$$\langle\overline{J_{3D}}\rangle=\frac{1}{A\Delta t}\int_t^{t+\Delta t}\int_A|\epsilon_{r\theta}|\left(1+\underbrace{\frac{\psi^2}{2}-\frac{\psi^4}{8}+\frac{\psi^6}{16}-\cdots}_{\text{higher order terms}}\right)dtdA \quad\cdots\cdots(27)$$

$$\psi=\frac{\sqrt{\dfrac{(\epsilon_\theta-I)^2}{2}+\dfrac{(\epsilon_r-I)^2}{2}+\dfrac{(\epsilon_z-I)^2}{2}+\epsilon_{zr}^2+\epsilon_{z\theta}^2}}{\epsilon_{r\theta}} \quad\cdots\cdots(28)$$

According to two dimensional visual test, we can expect the value of ψ is negligible since strains ϵ_r, ϵ_z, ϵ_θ, ϵ_{zr} and $\epsilon_{z\theta}$ are expected to be small compared with $\epsilon_{r\theta}$. Then, we have the representative of $\langle\overline{J}_{3D}\rangle$ as,

$$\langle\overline{J}_{1st,3D}\rangle=\frac{1}{A\Delta t}\int_A|\overline{\epsilon_{r\theta}}|\,dtdA=\frac{1}{A}\int_A\frac{1}{2}\left|\frac{1}{r}\frac{\overline{\partial u_r}}{\partial\theta}+\frac{\overline{\partial u_\theta}}{\partial r}-\frac{\overline{u_\theta}}{r}\right|dA$$

$$=\frac{1}{A}\int_{-\frac{d}{2}}^{\frac{d}{2}}\int_{r_1}^{r_2}\frac{1}{2}\left|\frac{\overline{u_\theta}}{r}\right|drdz \quad\cdots\cdots(29)$$

Since the variation of circumferential velocity across the pipe section is negligible, $\overline{u_\theta}$ can be replaced with sectional averaged circumferential velocity $\langle\overline{U}\rangle$ and the above expression can be rewrite as,

$$\langle\overline{J}_{1st,3D}\rangle=\frac{1}{2A}\langle\overline{U}\rangle\int_{-\frac{d}{2}}^{\frac{d}{2}}\int_{r_1}^{r_2}\frac{1}{r}\,drdz=\frac{1}{2A}\langle\overline{U}\rangle\int_{-\frac{d}{2}}^{\frac{d}{2}}\ln\left(\frac{r_2}{r_1}\right)dz \quad\cdots\cdots(30)$$

If the pipe radius with respect to z is large enough to assume,

$$\frac{1}{d_r}\ln\frac{r_2}{r_1}=\frac{1}{R} \quad\cdots\cdots(31)$$

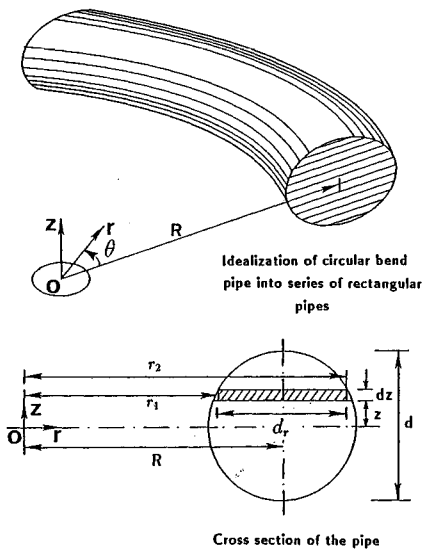

Fig. 21 Idealization of circular pipe into series of rectangular pipes.

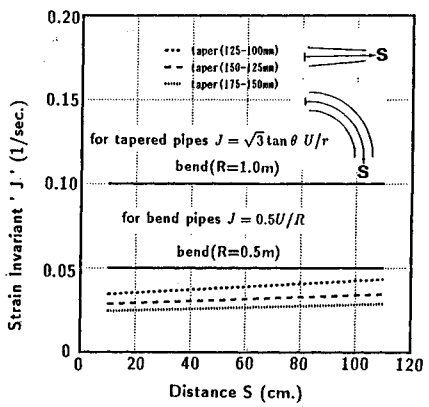

Fig. 22 Comparison of $\langle J\rangle$ values for bend and tapered pipes.

where $d_r = r_2 - r_1$ and $R = \dfrac{r_1 + r_2}{2}$, we have the same compatibility as in two dimensional case as follows.

$$\langle \overline{J}_{1st,3D} \rangle = \frac{1}{2A} \langle \overline{U} \rangle \int_{-\frac{d}{2}}^{\frac{d}{2}} \frac{d_r}{R} dz = \frac{1}{2} \frac{\langle \overline{U} \rangle}{R} \quad \cdots\cdots (32)$$

The compatibility relationship obtained for tapered pipes[7] is given as,

$$\langle \overline{J} \rangle = \frac{\sqrt{3}}{r} \tan\theta \langle U \rangle \quad \cdots\cdots (33)$$

where r is the radius of the pipe section concerned and θ is the tapered angle.

Comparing the compatibility obtained for tapered pipe[7] as given by Eq. (33) with that for bend pipe (Eq. (32)), it is clear that the shear deformational intensity is higher for bend pipes than for tapered pipe as indicated in Fig. 22.

The dimensions of bend and tapered pipes considered in calculating $\langle \overline{J} \rangle$ are the ones given in "Recommended Practice for Pumping Concrete"[1].

For the pipes considered in the recommended practice for concrete pumping, if the stiffness of the fresh concrete is same, the pressure drop across bend pipe is higher than that of tapered pipes and the ratio of the pressure drop between bend and tapered pipes varies according to the dimension of each part as indicated in Fig. 22. In case of tapered pipes, the pressure drop depends not only on the shear deformation of fresh concrete but also on the resistance due to the pipe wall reaction which is considered to be small in bend pipes.

6. CONCLUSIONS

By using flow visualization and image processing technique, a one-dimensional compatibility for deformation of particle assembly in bend pipe, which relates the mean speed of particles to the shear rate intensity of the particle assembly denoted by the second invariant of strain rate, was proposed. By combining the compatibility proposed in this research with the constitutive law for particle assembly, it is possible to complete the multi-phase dynamic model for fresh concrete which can be applied in bend pipes. The followings were experimentally and analytically clarified by results of the flow visualization test using model concrete.

(1) The deformation of particle assembly of liquid-solid flow in bend pipes is under pure shear deformation in which radial and circumferential strains are nearly equal to zero.

(2) In a two-dimensional bend pipe flow of dense liquid-solid, the sectional averaged intensity of shear rate is dependent on the mean particle speed and curvature of the bend, but hardly dependent on the liquid viscosity. For small curvatures, averaged shear intensity does not depend on the volume fraction of particles.

(3) The sectional averaged intensity of particles' shear rate was represented by the second invariant of strain rate, which was analytically integrated over a pipe section. The first order linear term of shear rate intensity was experimentally found to be prominent in comparison with the higher order term.

(4) The first linear term of deformational compatibility for particle assembly is theoretically derived from the mean flow speed and radius of curvature of the bend pipe.

ACKNOWLEDGMENTS

The authors are grateful to Prof. Hajime Okamura (University of Tokyo) for his valuable suggestions in connection with this work. The help of Mr. N. Okamura, an undergraduate student, in carrying out the experiment and analysis is also acknowledged. The authors express their gratitude to the Ministry of Education for providing financial support under the Grant-in-Aid for Scientific Research No. 0142003.

REFERENCES

1) Hashimoto, C., Maruyama, K. and Shimizu, K. : Electric Measurement System for Prediction of Blocking of Fresh Concrete Flowing in Pipes, Proceedings of the 3 rd International Symposium on Liquid-Solid Flows, Fed-Vol. 75, ASME, pp. 189-194, 1988.

2) Working Group on Recommendation for Pumping Methods in the Subcommittee on Construction Practice of JSCE : Recommended Practice for Pumping Concrete, Concrete Library of JSCE, No. 8, pp. 4-34, December 1986.

3) Wallis, G. B. : One Dimensional Two-Phase flow, McGraw-Hill, New York, 1969.

4) Roco, M. C. and Shook, C. A. : New Approach to Predict Concentration Distribution in Fine Particle Slurry Flows, PCH Physiochemical Hydrodynamics, Vol. 8, No. 1, pp. 43-60, 1987.

5) Nanayakkara, A., Ozawa, K., Gunatilaka, D. and Maekawa, K. : Two-Phase Computational Model for Flow and Segregation of Fresh Concrete in Tapered Pipes, Proceedings of the 3 rd International Symposium on Liquid-Solid Flows, ASME, pp. 47-52, 1988.

6) Ozawa, K., Nanayakkara, A. and Maekawa, K. : Flow and Segregation Behavior of Two-Phase Model Concrete Around Bifurcation in Pipe Lines, Proc. of JSCE, No. 408/V-11, pp. 195-203, August 1989.

7) Nanayakkara, A., Ozawa, K. and Maekawa, K. : Deformational Compatibility of Aggregate Phase For Tapering Flow of Dense Liquid-Solid Material, Proc. of JSCE, No. 420/V-13, pp. 279-290, August 1990.

8) Cundall, D. A. and Starck, O. D. L. : A Discrete Numerical Model for Granular Assemblies, Geotechnique 2, pp. 47-65, 1979.

9) Tanigawa, Y., Mori, H., Watanabe, K. and Miwa, M. : Suspension Element Analysis for Flow of Fresh Concrete in Tapered Pipe, Proc. of JCI, Vol. 11, No. 1, pp. 727-732, July, 1989.

10) Tarumi, Y. and Hakuno, M. : A Granular Assembly Simulation for the Liquefaction of Sand and Quick Sand, Bull. Earthq. Res. Inst., University of Tokyo, Vol. 62, pp. 535-577, 1987.

11) Ma, D. A. and Roco, M. C. : Probabilistic Three-Dimensional Model for Slow Shearing Particulate Flow : Wet Friction, Proc. of Third International Symposium on Liquid-Solid Flows, ASME, pp. 53-58, 1988.

12) Hashimoto, C., Maruyama, K. and Shimizu, K. : Study on Visualization of Blocking of Fresh Concrete Flowing in Pipe, Concrete Journal, Vol. 26, No. 2, pp. 119-127, February, 1988.

13) Ozawa, K., Nanayakkara, A. and Maekawa, K. : Evaluation of aggregate particle motion in liquid-solid flows of model concrete, Proc. of JSCE, No. 408/V-11, pp. 187-193, August 1989.

(Received April 26 1990)